Retention of Conformational Flexibility in HIV-1 Rev−RNA Complexes†

Thomas A. Wilkinson,‡,§ Lingyang Zhu,‡,|| Weidong Hu,‡ and Yuan Chen*,‡

Division of Immunology, Beckman Research Institute of the City of Hope National Medical Center, Duarte, California 91010

Received July 27, 2004; Revised Manuscript Received October 5, 2004

ABSTRACT: Sequence-specific recognition between HIV-1 Rev and viral RNA mediates the nuclear export of the viral mRNA and thus is important for the viral life cycle. HIV Rev binds to its viral RNA target with high affinity and specificity and also binds to an *in vitro* selected RNA aptamer that has a significantly different sequence from the viral RNA target with a 6-fold higher affinity than its natural target. The high-resolution structures of HIV Rev Arg-rich motif (ARM) in complexes with the wild-type RNA and the RNA aptamer reveal that, despite the significantly different RNA sequences, the two complexes share similar structural features and the protein−RNA interactions are mediated mostly by the Arg side chains in Rev ARM. To gain further insight into the role of these Arg side chains in the sequence-specific protein−RNA recognition, we have characterized the flexibility of these Arg side chains at the interfaces of the two high-affinity complexes using ^{15}N R_1, R_2, nuclear Overhauser effect, and chemical-shift anisotropy dipolar cross-correlation relaxation measurements. The ARM peptide contains uniformly $^{13}C/^{15}N$-labeled Arg residues, and the RNA samples were unlabeled. Despite the apparently similar roles of Arg side chains in both complexes, most of them display a different dynamic behavior in the context of different RNA molecules, and extensive and highly diverse motions have been observed for all of these side chains that interact with RNA. Most of the differences in side-chain dynamics between the complexes cannot be inferred from the three-dimensional structures. Additionally, more than half of the residues have increased flexibility in the Rev−RNA aptamer complex that has a higher affinity. This study provides new insights into ARM−RNA recognition and indicates that retention of conformational flexibility is likely important in high-affinity ARM−RNA recognition.

Rev is an essential virally encoded protein that is expressed during the early stages of human immunodeficiency virus type-1 (HIV-1)[1] replication and mediates the transport of singly spliced and unspliced viral mRNA out of the nucleus and into the cytoplasm of infected cells by binding to the Rev response element (RRE) of the viral RNA (*1*). Biochemical and genetic studies have shown that Rev 34−50 (Figure 1a) contains an arginine-rich motif (ARM) that is responsible for specific, high-affinity interactions (i.e., K_d in the nanomolar range) with RNA. Such studies have also determined that a stem-loop structure, stem-loop IIB (SLIIB, Figure 1b), within the RRE is both necessary and sufficient for specific, high-affinity interactions with Rev (*1*). Systematic evolution of ligands by exponential amplification (SELEX) (*2*) experiments have generated RNA aptamers that selectively bind the HIV-1 Rev ARM with high specificity and affinity, and one of these aptamers (Figure 1c) has higher affinity for the HIV-1 Rev than the wild-type SLIIB sequence (*3*). Rev-targeting aptamers have been found that can functionally substitute for SLIIB in Rev-mediated RNA export from the nucleus (*4*), indicating their suitability for use in RNA decoy strategies to block HIV replication *in vivo*. Accordingly, studies using RNA aptamers to disrupt the HIV-1 Rev−SLIIB interaction and inhibit viral replication via gene therapy approaches have been actively pursued (*4*−*8*).

Structural studies of a peptide corresponding to the Rev ARM sequence bound to either SLIIB (Figure 1b) or an RNA aptamer (Figure 1c), which has approximately a 6-fold higher affinity for HIV-1 Rev than the wild-type SLIIB sequence, demonstrate that the two peptide−RNA complexes share similar structural features (*9*, *10*). The ARM peptide forms an α helix that binds deeply within a widened major groove of an RNA hairpin structure. All of the peptide−RNA contacts are mediated by amino acid side chains, mostly the 10 Arg side chains, in both structures. The availability of the structures for the Rev ARM−SLIIB and aptamer complexes provides a compelling opportunity to investigate the molecular mechanism for high-affinity binding of Rev ARM to two distinct RNA targets. To understand the role of conformational flexibility in specific, high-affinity Rev ARM recognition of target RNA, the arginine side-chain dynamical behavior in the Rev ARM−aptamer complex was measured and compared to that found in the Rev ARM−SLIIB complex (*11*).

MATERIALS AND METHODS

Sample Preparation. A 35-nucleotide RNA oligomer corresponding to the RNA aptamer sequence (Figure 1c) was

† This work was supported by NIH Grant GM54190 (to Y.C.).

* To whom correspondence should be addressed. E-mail: ychen@coh.org. Telephone: (626) 930-5408. Fax: (626) 301-8186.

‡ Beckman Research Institute of the City of Hope National Medical Center.

§ Current address: Department of Molecular and Medical Pharmacology, University of California−Los Angeles, Los Angeles, CA 90095.

|| Current address: Array BioPharma Inc., Boulder, CO 80301.

[1] Abbreviations: HIV-1, human immunodeficiency virus type 1; CSA, chemical-shift anisotropy; HSQC, heteronuclear single-quantum correlation; ARM, Arg-rich motif; SLIIB, stem-loop IIB; RRE, Rev response element; NOE, nuclear Overhauser effect; TOCSY, total correlation spectroscopy.

10.1021/bi048409e CCC: $27.50
Published on Web 12/03/2004

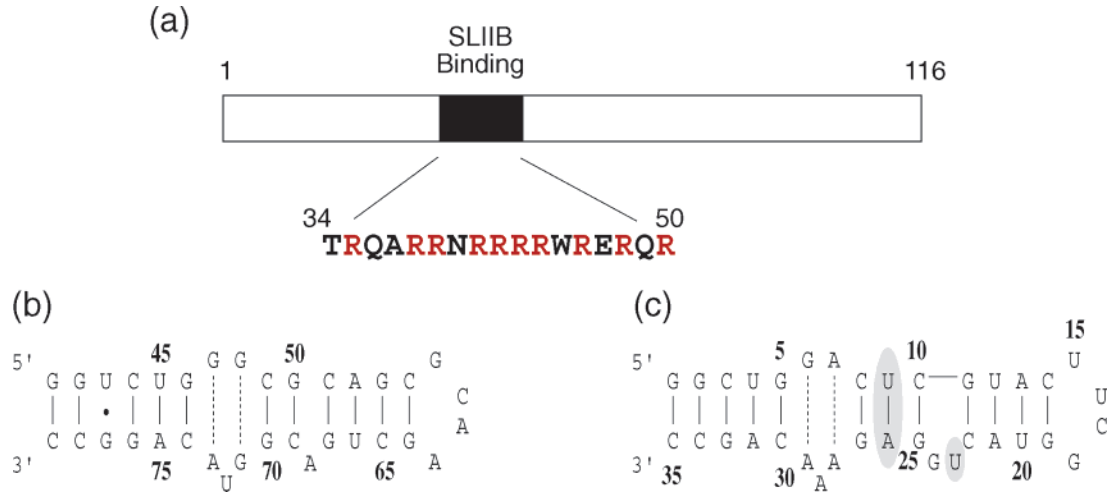

FIGURE 1: (a) HIV-1 Rev ARM sequence. The 10 Arg residues are indicated in red. (b) RNA sequence and numbering scheme corresponding to SLIIB. (c) High-affinity RNA aptamer sequence.

synthesized using *in vitro* T7 RNA polymerase transcription reactions and purified by gel electrophoresis using methods previously described (*11*). An equimolar amount of the ARM peptide [labeled as described previously (*11*)] was then added to unlabeled RNA aptamer to give a final Rev peptide/RNA aptamer complex concentration of 1.4−1.9 mM in 10 mM sodium phosphate buffer at pH 6.0. The NMR sample for the Rev ARM peptide/SLIIB complex was prepared as described (*11*).

NMR Spectroscopy and Resonance Assignments. All NMR experiments were performed at 25 °C and at a magnetic field of 11.7 T using either a Varian or a Bruker 500 MHz spectrometer equipped with four channels, pulse-shaping capabilities, and pulsed-field-gradient (PFG) hardware. To obtain the assignments of 10 arginine $^{15}N^{\epsilon}-^{1}H^{\epsilon}$ signals in the Rev ARM−aptamer complex (Arg 35, 38, 39, 41−44, 46, 48, and 50; Figure 2a), $^{15}N-^{1}H$ heteronuclear single-quantum coherence (HSQC) experiments (*12*), Arg-(H)C(C) total correlation spectroscopy (TOCSY), and Arg-H(CC) TOCSY experiments (*13*) were performed. The Arg-(H)C(C) TOCSY (*13*) experiment correlating the arginine H^{ϵ} proton with the side-chain carbons was performed using 64 t_1 increments of 2048 complex points (512 scans/increment) with spectral widths of 4500 and 12000 Hz (oversampling) in the ^{13}C and ^{1}H dimensions. The Arg-H(CC) TOCSY experiment (*13*) correlating the arginine H^{ϵ} proton with side-chain protons was executed using 38 t_1 increments having 2048 complex points (896 scans/transient) and spectral widths of 9 and 24 ppm in the F_1 and F_2 dimensions, respectively. The number of indirect dimension increments was extended to 76 by linear prediction. Proton pulses for these Arg-TOCSY experiments were centered at the water resonance, while carbon pulses were centered at 43.4 ppm. ^{15}N pulses were set to 100 ppm prior to the FLOPSY-8 sequence element, applied with a 9 kHz field, and then shifted to 81.5 ppm following FLOPSY transfer. Both Arg-TOCSY experiments used a 1 s recycle delay and employed DIPSI-2 mixing times of 74 ms for $C^{\delta} \rightarrow N^{\epsilon}$ magnetization transfer, with FLOPSY-8 mixing times of either 23 or 15 ms used for Arg-(H)C(C) TOCSY and Arg-H(CC) TOCSY experiments. The HNCA experiment was performed basically as previously described (*14*), with the pulse sequence being modified by removing the constant-time element and introducing a shaped pulse to decouple C^{β} nuclei, allowing an increased number of increments in the indirect dimension to be acquired. Observed chemical shifts from these experiments were compared with an assignment list for ^{1}H nuclei in the Rev peptide−RNA aptamer complex (*10*). Assignments of 7 well-resolved arginine amide signals (Arg 35, 38, 39, 41, 43, 44, and 46) in HSQC spectra were based upon data from the above experiments in conjunction with data from HNHA (*15*) and HNCA (*14*) experiments. The HNCA experiment was executed using 80 t_1 increments having 1504 complex points (192 transients/increment) with spectral widths of 20 and 12 ppm in the ^{1}H and ^{13}C dimensions, respectively, with ^{13}C and ^{15}N pulses set to 58 and 118 ppm, respectively. The HNHA experiment was performed as previously described (*16*) using 68 t_1 increments having 1504 complex points (256 scans/increment) with spectral widths of 1500 and 10000 Hz in the F_1 and F_2 dimensions, respectively; ^{13}C and ^{15}N pulses were set to 57 and 118 ppm, respectively. Proton pulses were placed at the water resonance for both HNCA and HNHA experiments. Unambiguous assignments of Arg 35, 42, and 44 signals were further confirmed through inspection of HSQC spectra of Rev ARM peptide−RNA aptamer complexes, where arginine ^{15}N-labeling was specifically introduced at Arg 35/Arg 42 or Arg 35/Arg 44 positions.

^{15}N T_1 and T_2 relaxation measurements and ^{15}N steady-state NOE measurements were performed using published pulse sequences (*17*). ^{15}N R_1 values were obtained from spectra that were acquired using relaxation delays of 85*, 340, 510, 680, 850*, 1020, and 1530 ms, and ^{15}N R_2 values were obtained from spectra that were recorded using Carr−Purcell−Meiboom−Gill (CPMG) periods of 16.8*, 33.5, 50.3, 67.1*, 83.8, 117.4, and 150.9 ms. Duplicated spectra are indicated by an asterisk. NOE spectra were acquired with and without a 3 s proton saturation period consisting of a series of 120° pulses applied every 5 ms; such spectra were collected in duplicate. A 2 s recovery period preceded the 3 s saturation period in NOE experiments where such saturation was employed, whereas a 5 s recovery period was used in NOE experiments that were acquired without saturation. Recovery delays of 2 s were used in T_1 and T_2 experiments. R_1, R_2, and NOE spectra were acquired with 28 t_1 increments of 1504 complex data points and using spectral widths of

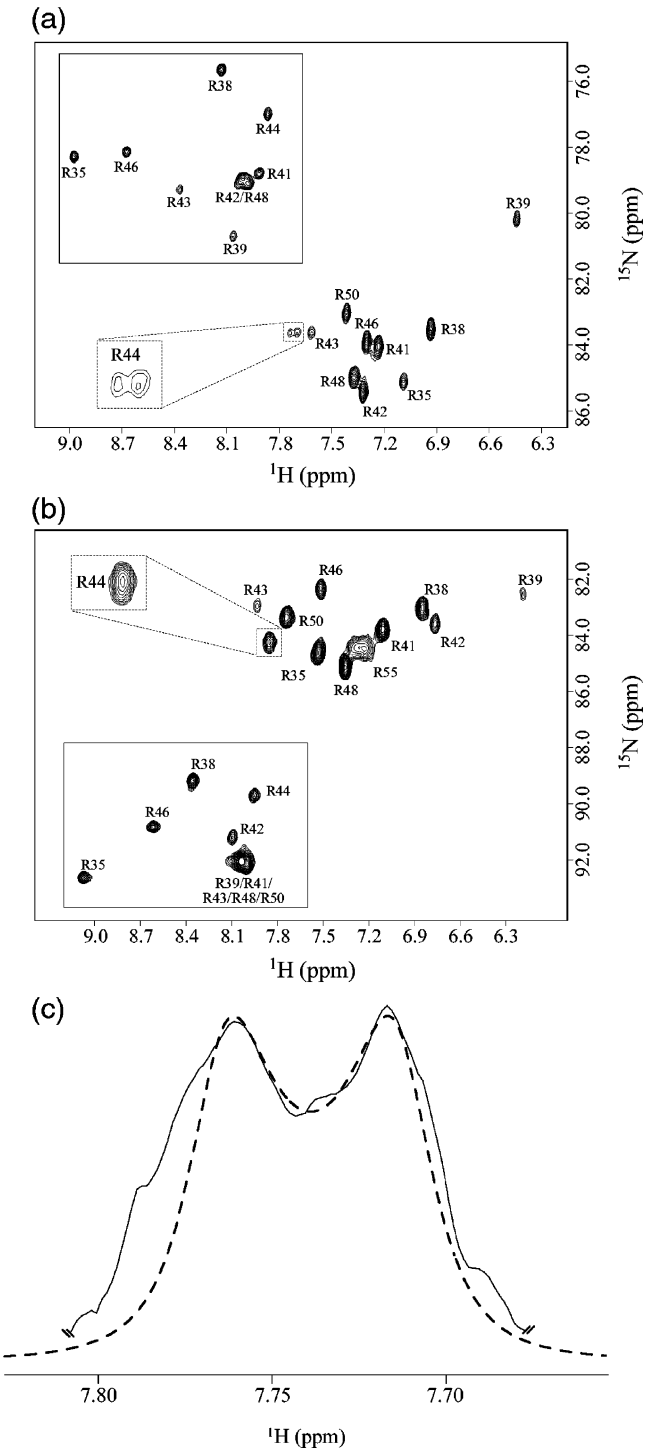

FIGURE 2: (a) Arg ϵ-nitrogen signals from a representative ^{1}H-^{15}N correlation spectrum of the Rev ARM peptide in complex with an RNA aptamer (25 °C, pH 6.0, and 11.7 T). (b) Arg ϵ-nitrogen signals from the Rev ARM peptide in complex with SLIIB (25 °C, pH 5.5, and 11.7 T). The Arg amide signals in each complex are boxed, and the Arg 44 $N^{\epsilon}-H^{\epsilon}$ signals are shown in enhanced detail within the dashed insets. (c) Superposition of the simulated line shape and actual 1D trace of the Arg44 side-chain ϵ-NH group.

500 and 10 000 Hz in the F_1 and F_2 dimensions, respectively. All spectra were processed using FELIX 98 (Accelrys). Uncertainties in peak height measurements were estimated by comparing peak heights from corresponding peaks in duplicate spectra as described previously (*11*). The average percent uncertainties in R_1, R_2, and NOE values for the ^{15}N nuclei were found to be 4.5, 3.8, and 10.9%, respectively. Transverse dipolar-chemical-shift anisotropy (CSA) cross-correlation (η_{xy}) experiments were performed with the pulse sequence described previously (*18*) using cross-correlation delays (4Δ) of 10, 15, 20, and 25 ms, along with a reference spectrum. The transverse dipolar-CSA cross-correlation experiment using the 20 ms delay was performed in duplicate for error analysis purposes.

The transverse dipolar-CSA cross-correlation effect builds up in the η_{xy} experiment according to the following function (*18*):

$$I_{cross}/I_{ref} = -\frac{e^{-4\eta_{xy}\Delta} - e^{4\eta_{xy}\Delta}}{e^{-2\eta_{xy}\delta} + e^{2\eta_{xy}\delta}} \quad (1)$$

where δ is a refocusing delay of $1/4J_{NH}$ in the η_{xy} reference experiment. The ratio in eq 1 above can be expressed as

$$I_{cross}/I_{ref} = -\frac{1}{2}(e^{-4\eta_{xy}\Delta} - e^{4\eta_{xy}\Delta}) \quad (2)$$

for $1 \leq \eta_{xy} \leq 25\ s^{-1}$ and $\delta = 2.65$ ms (as was employed in the reference experiment). Peak intensities from the reference and cross experiments were normalized according to the number of scans acquired in each experiment, and Curvefit (provided by Dr. Arthur G. Palmer, III) was used to fit the ratios of the normalized intensities to the function in eq 2 to generate estimates for η_{xy}. Curvefit was also used to calculate uncertainties in η_{xy} values, which were found to be 7.8 and 11.6% for η_{xy} of Arg side chains in complexes with the aptamer and SLIIB, respectively.

Reduced Spectral Density Mapping Calculations. The reduced spectral density mapping approach for estimating spectral density functions of $^{15}N-^{1}H$ bond vectors has been discussed in detail elsewhere (*19*, *20*). Expressions for the spectral density functions $J(0)$, $J(\omega_N)$, and $J(\omega_H)$ in terms of R_1 (longitudinal) and R_2 (transverse) autocorrelation rates and steady-state NOE values are given by eqs 5−7 in Farrow et al. (*20*) and are recapitulated here for the convenience of the reader (R_1 and R_2 are expressed as $1/T_1$ and $1/T_2$, respectively). Under the assumption that $J(\omega_H \pm \omega_N) \approx J(\omega_H)$

$$J(\omega_H) = \frac{4}{5d^2}\frac{\gamma_N}{\gamma_H}\frac{(NOE - 1)}{T_1} \quad (3)$$

$$J(\omega_N) = \frac{\left[\frac{1}{T_1} - \frac{7d^2}{4}J(\omega_H)\right]}{\frac{3d^2}{4} + c^2} \quad (4)$$

$$J(0) = \frac{\left[\frac{1}{T_2} - \left(\frac{3d^2}{8} + \frac{c^2}{2}\right)J(\omega_N) - \left(\frac{13d^2}{8}\right)J(\omega_H)\right]}{\frac{d^2}{2} + \frac{2c^2}{3}} \quad (5)$$

where $d = [\{\mu_0 h\gamma_N\gamma_H/8\pi^2\}/\langle r_{NH}^3\rangle]$, $c = \omega_N\Delta\sigma/\sqrt{3}$, μ_0 is the permeability of free space, h is Plank's constant, γ_N and γ_H are the gyromagnetic ratios of the ^{15}N and ^{1}H nuclei, respectively, r_{NH} is the $^{15}N-^{1}H$ internuclear distance, and $\Delta\sigma$ is the difference between the parallel and perpendicular components of the CSA tensor. Values for $J(0)$ in eq 5 above were calculated for $^{15}N-^{1}H$ bond vectors from the experi-

mentally determined R_1, R_2, and NOE values. The transverse dipolar-CSA cross-correlation rate (η_{xy}) is related to the spectral density by

$$\eta_{xy} = \frac{\sqrt{3}}{6} cdP_2(\cos\theta)[4J^{cc}(0) + 3J(\omega_N)] \qquad (6)$$

where θ is the angle between the $^{15}N-^{1}H$ bond vector and the principal axis of the ^{15}N chemical-shift tensor, assumed to be axially symmetric, and $P_2(x) = (3x^2 - 1)/2$. The $J^{cc}(0)$ term derived from the measured η_{xy} parameter is free from contributions from micro- to millisecond chemical-exchange processes, whereas $J(0)$ calculated from R_1, R_2, and NOE parameters may include contributions from chemical exchange (*21*). A qualitative comparison of $J(0)$ and $J^{cc}(0)$ values for the various arginine $^{15}N-^{1}H$ bond vectors allowed identification of arginine side-chain and backbone groups that are subject to micro- to millisecond exchange processes. Calculations of $J(0)$ and $J^{cc}(0)$ employed $\Delta\sigma$ and θ values of -160 ppm and $-20°$, respectively. Substitution of other values for $\Delta\sigma$ (-120 and -200 ppm) and θ ($10-35°$) resulted in uniform changes in $J(0)$ and $J^{cc}(0)$ that did not alter the final assessment of the relative mobility of arginine side chains when bound to either SLIIB or aptamer RNA. Uncertainties in calculated spectral density function values were derived using the error formula

$$\Delta J(0) = \left[\sum_{i=1}^{3}\left(\frac{\partial J(0)}{\partial x_i}\right)^2 (\Delta x_i)^2\right]^{1/2} \qquad (7)$$

where the $x_{1,2,3}$ represent either the ^{15}N R_1, R_2, and NOE relaxation parameters [when estimating $\Delta J(0)$] or the ^{15}N R_1, NOE, and η_{xy} parameters [when estimating $\Delta J^{cc}(0)$].

Line-Shape Analysis. Analysis of the Arg 44 N^{ϵ} line shape to estimate the exchange rate between two Arg 44 side-chain conformations was performed using a Mathematica script that simulates line shapes according to the two-site exchange model described by Rogers and Woodbrey (*22*). Each site was assumed to be similarly populated and to have equivalent R_2 relaxation rates. Iterative fitting of the simulated line shape to the actual line shape was performed by varying both the exchange rate and the chemical-shift difference between each site (in the absence of exchange) until an optimal match between simulated and actual line shapes was achieved (Figure 2c).

RESULTS

Resonance Assignments. Assignments of 10 arginine $^{15}N^{\epsilon}-^{1}H^{\epsilon}$ signals in the Rev ARM−aptamer complex (Arg 35, 38, 39, 41−44, 46, 48, and 50) were achieved using Arg-(H)C(C) TOCSY and Arg-H(CC) TOCSY experiments (*13*) that correlate the arginine H^{ϵ} proton with either arginine side-chain carbon or proton chemical shifts. Observed chemical shifts from these experiments were compared with an assignment list for ^{1}H nuclei in the Rev peptide−RNA aptamer complex (*10*). Assignments of 7 well-resolved arginine backbone amide signals (Arg 35, 38, 39, 41, 43, 44, and 46) were based upon data from the above experiments in conjunction with data from HNHA (*15*) and HNCA (*14*) experiments. Unambiguous assignments of Arg 35, 42, and 44 signals were further confirmed through inspection of HSQC spectra (*12*) of Rev ARM peptide−RNA aptamer complexes, where arginine ^{15}N labeling was specifically introduced at Arg 35/Arg 42 or Arg 35/Arg 44 positions. The assignments of both the backbone amide NH and side-chain ϵ-NH groups are indicated in the HSQC spectra (Figure 2a). Assignments of backbone amide NH and side-chain ϵ-NH groups in the Rev ARM−SLIIB complex (Figure 2b) were made as previously described (*11*). The side-chain ϵ-NH group of Arg 44 splits into two peaks, which indicate that a conformational exchange process occurs on the time scale of millisecond to second.

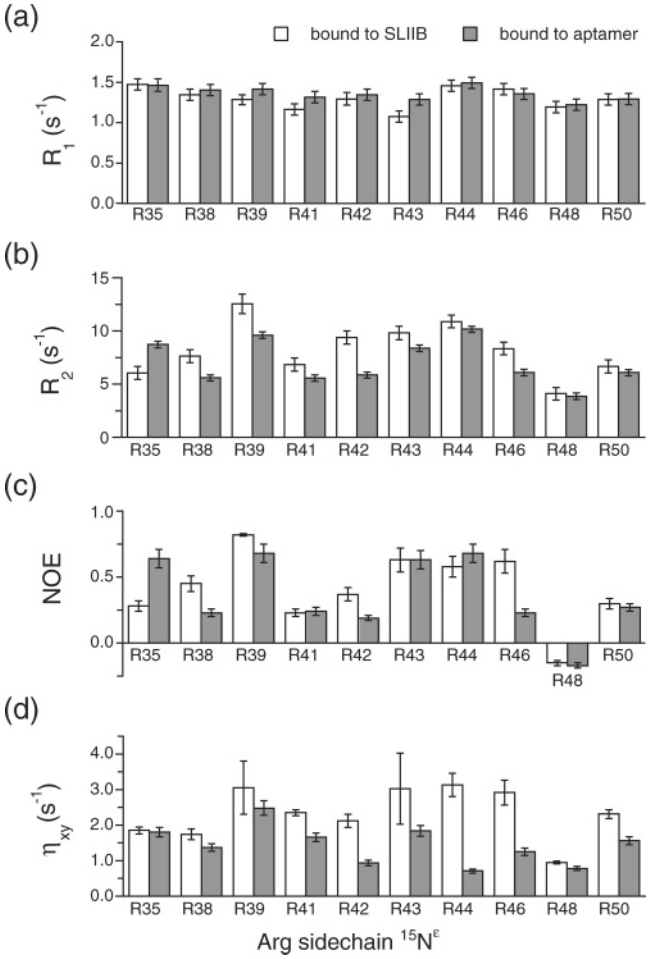

FIGURE 3: (a−d) R_1, R_2, steady-state NOE, and η_{xy} data for Arg side-chain $^{15}N^{\epsilon}$ nuclei. ^{15}N T_1 and T_2 relaxation measurements, ^{15}N steady-state NOE measurements, and the transverse dipolar-CSA cross-correlation experiments were performed as described in the Materials and Methods.

^{15}N Relaxation Measurements. Arginine backbone and side-chain dynamics in the Rev ARM−aptamer complex were characterized via ^{15}N relaxation measurements using a peptide corresponding to Rev ARM (residues 34−50) having ^{13}C-^{15}N-labeled arginine residues incorporated by chemical synthesis as described previously (*11*). The backbone amide and side-chain ϵ-NH groups were used as probes for backbone and side-chain dynamics, respectively. All 10 side-chain ϵ-NH groups are resolved in the ^{1}H-^{15}N HSQC spectrum for the Rev ARM−aptamer complex (Figure 2a). Measurements of R_1, R_2, and $^{15}N\{^{1}H\}$ steady-state NOE values (*17*) for the arginine ^{15}N amide and $^{15}N^{\epsilon}$ nuclei in the Rev ARM−RNA aptamer complex were performed under conditions similar to those used previously for the characterization of the Rev ARM−SLIIB complex (*11*), allowing a straightforward comparison of Rev arginine side-chain

Table 1: R_1, R_2, NOE, and η_{xy} Relaxation Parameters for Arginine Amide ^{15}N Nuclei in the Rev ARM−SLIIB and ARM−RNA Aptamer Complexes

amide ^{15}N nucleus	Arg	R_1 (s^{-1})	R_2 (s^{-1})	NOE	η_{xy} (s^{-1})
bound to SLIIB	35	1.47 ± 0.07	13.01 ± 0.57	0.70 ± 0.10	8.42 ± 0.33
	38	1.52 ± 0.07	12.15 ± 0.61	0.77 ± 0.11	8.76 ± 0.34
	42	1.29 ± 0.07	13.97 ± 0.60	0.84 ± 0.12	7.34 ± 0.53
	44	1.41 ± 0.08	12.97 ± 0.67	0.83 ± 0.12	8.85 ± 0.52
	46	1.55 ± 0.07	11.32 ± 0.63	0.57 ± 0.08	8.20 ± 0.42
bound to aptamer	35	1.47 ± 0.07	11.06 ± 0.30	0.72 ± 0.08	6.75 ± 0.12
	38	1.64 ± 0.07	11.40 ± 0.30	0.72 ± 0.08	7.24 ± 0.18
	39	1.66 ± 0.07	10.75 ± 0.31	0.79 ± 0.09	6.71 ± 0.14
	41	1.49 ± 0.07	11.72 ± 0.30	0.77 ± 0.08	7.89 ± 0.15
	43	1.64 ± 0.08	11.25 ± 0.30	0.74 ± 0.08	6.74 ± 0.13
	44	1.70 ± 0.07	11.18 ± 0.30	0.73 ± 0.08	7.21 ± 0.13
	46	1.62 ± 0.07	11.74 ± 0.29	0.70 ± 0.08	6.89 ± 0.17

dynamics in the context of different RNA targets. The CSA-dipolar cross-correlation η_{xy} values (*18*, *21*) were also measured for both complexes using identical experimental parameters to make a direct comparison. A comparison of the 10 arginine $^{15}N^{\epsilon}$ R_1, R_2, steady-state NOE, and η_{xy} values in the Rev ARM−SLIIB and RNA aptamer complexes is shown in parts a−d of Figure 3. Owing to spectral overlap, only backbone amide ^{15}N relaxation parameters for Arg 35, 38, 44, and 46 could be compared (Table 1).

Differences in Arg Side-Chain Dynamics on the Pico- to Nanosecond Time Scale. Inspection of arginine $^{15}N\{^1H\}$ NOE values in the Rev ARM−SLIIB and ARM−aptamer complexes reveals a diverse range of pico to nanosecond side-chain mobilities (Figure 3c). As was found in the Rev ARM−SLIIB complex (*11*), the arginine side chains in the aptamer complex also show a wide variety of flexibilities on the pico to nanosecond time scale. NOE values for Arg $^{15}N^{\epsilon}$ in the ARM−aptamer complex range from −0.2 (Arg 48) to 0.7 (Arg 39 and 44). Conversely, the arginine backbone amide groups in both the Rev ARM−SLIIB and aptamer complexes are all fairly rigid, having amide ^{15}N NOE values of 0.7−0.8 (*23*) (Table 1).

Because the sizes of the two complexes are nearly identical and the shapes are very similar, a direct comparison of relaxation parameters provides information on similarities and differences of the dynamic behavior of each N−H group. Examination of the Arg $^{15}N^{\epsilon}-^1H^{\epsilon}$ relaxation parameters associated with either the aptamer or the SLIIB complexes indicates significant differences in the mobilities of individual arginine side chains. The Arg $^{15}N^{\epsilon}-^1H^{\epsilon}$ NOE values indicate that pico to nanosecond flexibilities of four of these side chains (Arg 38, 39, 42, and 46) are increased in the ARM−aptamer complex relative to that in the Rev ARM−SLIIB complex (Figure 3c). In addition, although the NOE values for the Arg 41 and Arg 43 side chains are very similar, the R_2 values for these side chains decrease and the R_1 values increase in the aptamer complex, relative to the values found in the SLIIB complex. This observation suggests that the flexibilities of Arg 41 and Arg 43 side chains may have slightly increased on the nanosecond time scale. In total, the pico to nanosecond flexibilities of six of these side chains (Arg 38, 39, 41−43, and 46) are increased in the ARM−aptamer complex relative to that in the Rev ARM−SLIIB complex. Conversely, the Arg 35 side chain is considerably less flexible in the aptamer complex than in the SLIIB complex, as the NOE values for the Arg 35 side chain increase from 0.28 ± 0.04 in the SLIIB complex to 0.64 ± 0.07 in the aptamer complex.

The differences in pico to nanosecond dynamics of the Arg side chains at the binding interfaces are not directly inferred from the three-dimensional structures, except for Arg 35. The relaxation behavior of the Arg 35 side chain is consistent with the structural data; in the ARM−aptamer complex, this side chain forms contacts with a U·AU base triple (*10*) that is not present in the ARM−SLIIB complex. The basis for the increase in dynamics of the side chains of Arg 38, 39, 41−43, and 46 is not obvious from an inspection of the NMR structures. For example, the NMR structures show that the Arg 46 side chain is similarly oriented toward noncanonical "S-shaped" phosphate backbone folds in both the ARM−SLIIB and ARM−aptamer complexes, but the dynamics of this side chain, as judged by R_2 and NOE values, are quite different depending upon the RNA context (parts b and c of Figure 3).

Differences in Arg Side-Chain Dynamics on the Micro- to Millisecond Time Scale. Assessment of the micro- to millisecond time-scale behavior (i.e., R_{ex}) of the various Arg side chains in the ARM−aptamer complex was obtained through measurements of $^{15}N^{\epsilon}$ CSA-dipolar cross-correlation rates (η_{xy}) (*18*, *21*) as described in the Materials and Methods. The same measurements were also performed for the Arg side chains in the ARM−SLIIB complex for comparison. The results of these measurements are shown in Figure 3d. Values for Arg $^{15}N^{\epsilon}$ η_{xy} range from 0.95 to 3.13 s^{-1} in the SLIIB complex and from 0.71 to 2.48 s^{-1} in the aptamer complex. The large variations of the η_{xy} values of the Arg side chains in complex with the aptamer and with SLIIB further demonstrate the diverse mobility of these side chains in complexes with both RNA molecules. The observed values for backbone amide ^{15}N η_{xy} in both complexes are significantly larger and more uniform than $^{15}N^{\epsilon}$ η_{xy} values (Table 1).

Spectral density function $J(0)$ was calculated from either R_1, R_2, and NOE or from R_1, η_{xy}, and NOE to obtain information about arginine side-chain conformational flexibilities on the micro- to millisecond time scale. R_2 relaxation rates are dominated by $J(0)$ contributions and are sensitive to micro- to millisecond dynamics, while η_{xy} values are dominated by $J^{cc}(0)$ and are not sensitive to chemical-exchange processes that occur on micro- to millisecond time scales. $J(0)$ values were estimated by using R_2, R_1, and NOE parameters (Figure 4a), and $J^{cc}(0)$ values were estimated from η_{xy}, R_1, and NOE values (Figure 4b) using eqs 1−4. In the absence of dynamics on the micro- to millisecond time scale, $J(0)$ and $J^{cc}(0)$ values will be similar. However, in the presence of micro- to millisecond dynamics, the $J(0)$ values

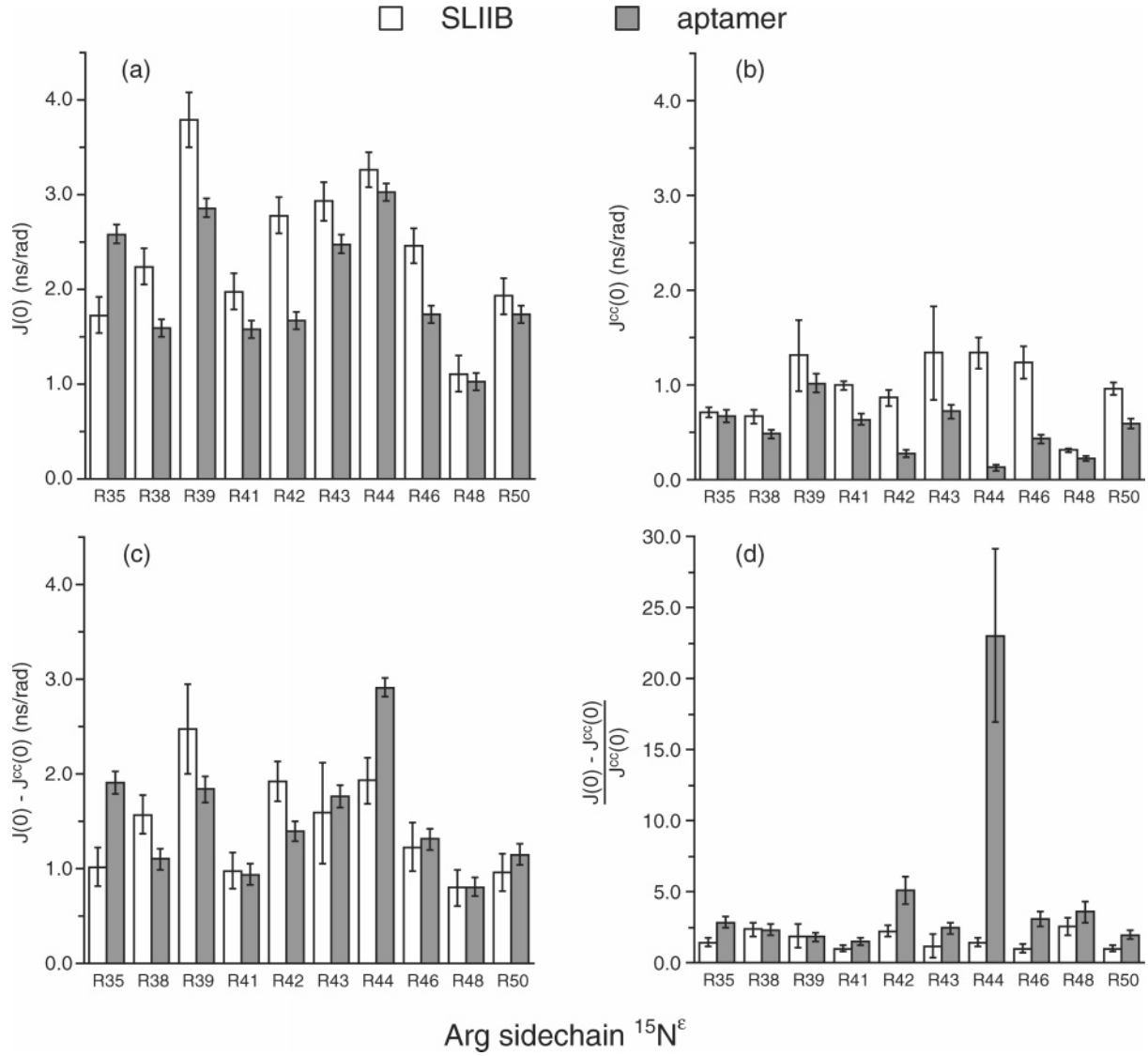

FIGURE 4: Dynamics on the micro- to millisecond time scale of each Arg side chain as indicated by $J(0)$ and $J^{cc}(0)$ in both peptide−RNA complexes. (a) $J(0)$ calculated from R_2, R_1, and steady-state NOE values. (b) $J^{cc}(0)$ calculated from η_{xy}, R_1, and steady-state NOE values. (c) Difference between $J(0)$ and $J^{cc}(0)$, $[J(0) - J^{cc}(0)]$, reflecting the chemical-exchange contribution of each Arg side chain. (d) Ratio $[J(0) - J^{cc}(0)]/J^{cc}(0)$ for each side chain in both complexes, indicating the relative contribution of chemical-exchange and dipolar-relaxation processes toward the transverse autorelaxation rate R_2.

estimated using R_2, R_1, and NOE relaxation rates will be larger than $J^{cc}(0)$, because R_2 values are larger because of chemical-exchange (R_{ex}) contributions. The differences between $J(0)$ and $J^{cc}(0)$ values $[J(0) - J^{cc}(0)]$ for arginine side chains in either the Rev ARM−SLIIB or ARM−aptamer complex (Figures 4c) indicate that the R_2 values of all 10 arginine side chains have R_{ex} contributions in both complexes. Therefore, all side chains experience micro- to millisecond exchange effects in both complexes to some extent.

The relative R_{ex} contribution toward the transverse autorelaxation rate R_2 was assessed by the ratio $[(J(0) - J^{cc}(0))/J^{cc}(0)]$ for each arginine side chain in the two complexes (Figure 4d). These results show that the contribution of micro- to millisecond motion toward R_2 is increased in the aptamer complex for Arg 35, 42, 44, 46, and 50 side chains. Most strikingly, the relative R_{ex} contribution associated with the Arg 44 $^{15}N^{\epsilon}-^{1}H^{\epsilon}$ bond vector in the aptamer complex indicates that micro- to millisecond motion of this side chain is nearly wholly responsible for the observed R_2 transverse relaxation rate. Such a significant contribution is consistent with the observation that the Arg 44 $^{15}N^{\epsilon}-^{1}H^{\epsilon}$ group in the aptamer complex generates two peaks of similar intensity in the $^{15}N-^{1}H$ HSQC spectrum (Figure 2a), indicating slow exchange on the chemical shift time scale between two similarly populated conformations. Analogous slow exchange behavior is not observed for the Arg 44 side chain in the Rev ARM−SLIIB complex (Figure 2b).

To obtain quantitative information on the slow conformational exchange of the Arg 44 side chain, line-shape analysis was performed using the two-site exchange formalism described by Rogers and Woodbrey (*22*). The dipolar contribution of R_2 in this fitting was estimated based on the measured R_2 values and the CSA-dipolar cross-relaxation rate. This analysis used a proton-shift difference of 29 Hz between the two component peaks and indicated that the exchange rate is approximately 43 s^{-1}. Superposition of the simulated and actual line shapes is shown in Figure 2c.

To gain further insight into the conformational exchange associated with the side chain of Arg 44, the NMR structure of the ARM−aptamer complex (archived in the Protein Data

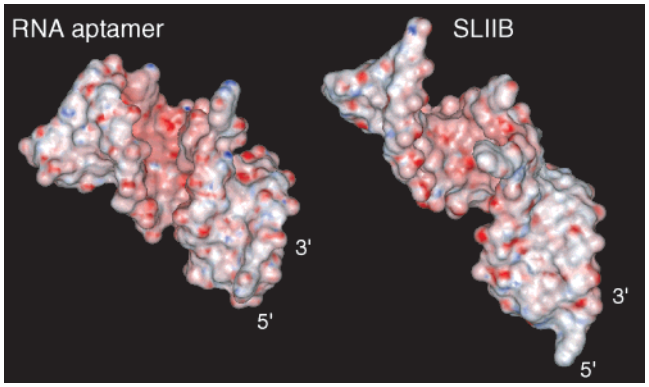

FIGURE 5: Mapping of the surface electrostatic potential of the RNA aptamer and SLIIB, with red indicating the negative charge and blue indicating the positive charge. The electrostatic potential was calculated using the AMBER force field within DELPHI (Accelrys).

Bank; PDB accession code 1ull) was inspected. In the ensemble of the seven NMR structures, it shows that the Arg 44 $^{15}N^{\epsilon}-^{1}H^{\epsilon}$ group is oriented toward Ura 4 in three of the structures, suggesting that the Arg 44 $^{15}N^{\epsilon}-^{1}H^{\epsilon}$ group forms a hydrogen bond with the O4 acceptor atom within this nucleotide (*10*). Conversely, the Arg 44 $^{15}N^{\epsilon}-^{1}H^{\epsilon}$ group is pointed away from the O4 atom of Ura 4 in the remaining four structures. This lack of precise positioning within the family of NMR structures further suggests that the Arg 44 side chain may sample different conformations in the Rev ARM−aptamer complex, with approximately 50% of the conformers forming a hydrogen bond with Ura 4. Collectively, the structural and dynamical data suggest that any hydrogen bond that is formed with Ura 4 is likely to be relatively transient in nature, being established and broken on a time scale that is slower than the microsecond range.

Electrostatic Potential Mapping of Target RNA. To further understand how flexible protein side chains might interact with RNA, surface electrostatic potentials of both SLIIB and the aptamer were evaluated. For both RNA molecules, the major grooves (the site of Rev ARM binding) have large areas of relatively uniform negative electrostatic potential (Figure 5), suggesting that most of the arginine side chains may be able to adopt different orientations without significant enthalpic penalties arising from the loss of electrostatic or hydrogen-bonding interactions. At the same time, by allowing conformational flexibility of Arg side chains at the interface, the entropic cost of the complex formation is mitigated [it has been estimated that complete restriction of arginine side-chain motion corresponds to an entropic penalty of approximately 2 kcal/mol (*24*)].

DISCUSSION

Side-Chain Flexibility Is Maintained at the High-Affinity Rev ARM−RNA Aptamer Interface. Both SLIIB and the RNA aptamer bind the Rev ARM with nanomolar affinity, with the aptamer binding the ARM with approximately 6-fold higher affinity than SLIIB (*3*). The two peptide−RNA complexes have similar structures despite the significant differences in the target RNA sequences. In both complexes, the Rev ARM forms an α helix that inserts deeply into the major groove of the RNA and the 10 Arg residues of Rev ARM are located at the binding interfaces and mediate most of the protein−RNA interactions. A common feature of the two high-affinity complexes is the extensive and highly diverse flexibility of the Arg side chains at the binding interfaces of both complexes. This observation suggests that extensive and diverse interfacial motion could be a general feature of Rev ARM interactions with other RNA aptamers. Conceivably, such dynamic behavior may be found at other protein ARM−RNA interfaces as well [for example, in bovine immunodeficiency virus (BIV) Tat−target RNA interactions]. Thus, side-chain flexibility is an important consideration in the theoretical prediction and design of RNA- and protein-binding sites based on ARM−RNA interaction.

The Higher-Affinity RNA Aptamer Complex Does Not Have a More Rigid Interface. In all, at least seven arginine side chains (Arg 38, 39, 41−44, and 46) experience increased mobility on either a pico- to nanosecond or micro- to millisecond time scale in the aptamer complex (relative to the SLIIB complex), while only one side chain (Arg 35) experiences reduced mobility on a pico- to nanosecond time scale. The entropic penalty incurred by conformational restriction of the Arg 35 side chain could be mitigated by increases in flexibility elsewhere in the complex. Indeed, the Arg 35 side chain itself displays some increased flexibility on the micro- to millisecond time scale in the aptamer complex. Furthermore, as this RNA aptamer binds Rev with a 6-fold higher affinity than the wild-type SLIIB sequence, the data suggest that higher affinity interactions do not necessarily lead to a uniform increase in rigidity at the binding interface. In fact, the contrary is observed here.

Implications on Entropic Contribution to Folding and Binding. Both protein-folding and protein-binding events are driven by similar forces, such as the hydrophobic effect, electrostatic interactions, and hydrogen bonding. However, the role of dynamics in protein folding and complex formation is not yet completely understood. Recent studies by deuterium NMR relaxation measurements indicate that significant side-chain motion exists within the protein hydrophobic core (*25*−*27*). Side-chain flexibility at interfaces has been observed in other protein−protein and protein−DNA complexes (*25*, *28*, *29*). In the study described here, the characterization of the dynamics of the majority of the side chains (arginine) at the protein−RNA-binding interfaces shows that higher affinity interactions do not necessarily lead to more rigidity at the binding interface, and thus, retention of conformational flexibility may be important in mitigating entropic penalty upon complex formation.

Advantages of folding upon binding have been previously suggested and include the control of binding specificity and affinity (*30*), the lowering of the energy barrier for complex formation (*31*), and the ability to bind multiple targets. Coupling folding to binding may also be important in distributing the information for affinity and specificity in the context of a three-dimensional structure, instead of encoding the information upon individual residues. In this way, random mutations can be better tolerated without detriment to the function. For example, although all Arg residues in Rev ARM form interactions with the RNA, substitutions of three of the Arg residues (Arg 41, 42, and 43) do not significantly affect the dissociation constant of the Rev ARM−SLIIB complex (*32*). Similarly, although the RNA aptamer has a significantly different sequence from SLIIB RNA, common three-dimensional structural features allow the aptamer to

bind the Rev ARM with high affinity and specificity. In folding upon binding processes, maintenance of conformational flexibility during complex formation is likely to be of general importance.

ACKNOWLEDGMENT

We thank Dr. Rafael P. Brüschweiler for helpful discussions and Dr. Robert E. London for helpful discussions and the Mathematica script for line-shape analysis.

REFERENCES

1. Pollard, V. W., and Malim, M. H. (1998) The HIV-1 Rev protein, *Annu. Rev. Microbiol. 52*, 491−532.
2. Brody, E. N., and Gold, L. (2000) Aptamers as therapeutic and diagnostic agents, *J. Biotechnol. 74*, 5−13.
3. Giver, L., Bartel, D., Zapp, M., Pawul, A., Green, M., and Ellington, A. D. (1993) Selective optimizaton of the Rev-binding element of HIV-1, *Nucleic Acids Res. 21*, 5509−5516.
4. Symensma, T. L., Giver, L., Zapp, M., Takle, G. B., and Ellington, A. D. (1996) RNA aptamers selected to bind human immunodeficiency virus type 1 Rev *in vitro* are Rev responsive *in vivo*, *J. Virol. 70*, 179−187.
5. Konopka, K., Lee, N. S., Rossi, J., and Düzgünes, N. (2000) Rev-binding aptamer and CMV promoter act as decoys to inhibit HIV replication, *Gene 255*, 235−244.
6. Good, P. D., Krikos, A. J., Li, S. X. L., Bertrand, E., Lee, N. S., Giver, L., Ellington, A., Zaia, J. A., Rossi, J. J., and Engelke, D. R. (1997) Expression of small, therapeutic RNAs in human cell nuclei, *Gene Ther. 4*, 45−54.
7. Inouye, R. T., Du, B., Boldt-Houle, D., Ferrante, A., Park, I.-W., Hammer, S. M., Duan, L., Groopman, J. E., Pomerantz, R. J., and Terwilliger, E. F. (1997) Potent inhibition of human immunodeficiency virus type 1 in primary T cells and aveolar macrophages by a combination anti-Rev strategy delivered in an adeno-associated virus vector, *J. Virol. 71*, 4071−4078.
8. Konopka, K., Duzgunes, N., Rossi, J., and Lee, N. S. (1998) Receptor ligand-facilitated cationic liposome delivery of anti-HIV-1 Rev-binding aptamer and ribozyme DNAs, *J. Drug Targeting 5*, 247−259.
9. Battiste, J. L., Mao, H., Rao, N. S., Tan, R., Muhandiram, D. R., Kay, L. E., Frankel, A. D., and Williamson, J. R. (1996) α Helix−RNA major groove recognition in an HIV-1 Rev peptide−RRE RNA complex, *Science 273*, 1547−1551.
10. Ye, X., Gorin, A., Ellington, A. D., and Patel, D. J. (1996) Deep penetration of an α-helix into a widened RNA major groove in the HIV-1 Rev peptide−RNA aptamer complex, *Nat. Struct. Biol. 3*, 1026−1033.
11. Wilkinson, T. A., Botuyan, M. V., Kaplan, B. E., Rossi, J. J., and Chen, Y. (2000) Arginine side-chain dynamics in the HIV-1 Rev−RRE complex, *J. Mol. Biol. 303*, 515−529.
12. Kay, L. E., Keifer, P., and Saarinen, T. (1992) Pure absorption gradient enhanced heternuclear single quantum correlation spectroscopy with improved sensitivity, *J. Am. Chem. Soc. 114*, 10663−10665.
13. Rao, N. S., Legault, P., Muhandiram, D. R., Greenblatt, J., Battiste, J. L., Williamson, J. R., and Kay, L. E. (1996) NMR pulse schemes for the sequential assignment of arginine side-chain H^{ϵ} protons, *J. Magn. Reson., Ser. B 113*, 272−276.
14. Yamazaki, T., Lee, W., Revington, M., Mattiello, D. L., Dahlquist, F. W., Arrowsmith, C. H., and Kay, L. E. (1994) An HNCA pulse scheme for the backbone assignment of ^{15}N, ^{13}C, ^{2}H-labeled proteins: Application to a 37-kDa *Trp* repressor−DNA complex, *J. Am. Chem. Soc. 116*, 6464−6465.
15. Vuister, G. W., and Bax, A. (1993) Quantitative *J* correlation: A new approach for measuring homonuclear three-bond $J(H^{N}H^{\alpha})$ coupling constants in ^{15}N-enriched proteins, *J. Am. Chem. Soc. 115*, 7772−7777.
16. Kay, L. E., Wittekind, M., McCoy, M. A., Friedrichs, M. S., and Mueller, L. (1992) 4D NMR triple-resonance experiments for assignment of protein backbone nuclei using shared constant-time evolution periods, *J. Magn. Reson. 98*, 443−450.
17. Farrow, N. A., Muhandiram, R., Singer, A. U., Pascal, S. M., Kay, C. M., Gish, G., Shoelson, S. E., Pawson, T., Forman-Kay, J. D., and Kay, L. E. (1994) Backbone dynamics of a free and phosphopeptide-complexed Src homology 2 domain studied by ^{15}N NMR relaxation, *Biochemistry 33*, 5984−6003.
18. Tessari, M., Mulder, F. A. A., Boelens, R., and Vuister, G. W. (1997) Determination of amide proton CSA in ^{15}N-labeled proteins using ^{1}H CSA/$^{15}N-^{1}H$ dipolar and ^{15}N CSA/$^{15}N-^{1}H$ dipolar cross-correlation rates, *J. Magn. Reson. 127*, 128−133.
19. Dayie, K. T., Wagner, G., and Lefèvre, J.-F. (1996) Theory and practice of nuclear spin relaxation in proteins, *Annu. Rev. Phys. Chem. 47*, 243−282.
20. Farrow, N. A., Zhang, O., Szabo, A., Torchia, D. A., and Kay, L. E. (1995) Spectral density function mapping using ^{15}N relaxation data exclusively, *J. Biomol. NMR 6*, 153−162.
21. Kroenke, C. D., Loria, J. P., Lee, L. K., Rance, M., and Palmer, A. G., III (1998) Longitudinal and transverse ^{1}H-^{15}N dipolar/^{15}N chemical shift anisotropy relaxation interference: Unambiguous determination of rotational diffusion tensors and chemical exchange effects in biological macromolecules, *J. Am. Chem. Soc. 120*, 7905−7915.
22. Rogers, M. T., and Woodbrey, J. C. (1962) A proton magnetic resonance study of hindered internal rotation in some substituted *N,N*-dimethylaminides, *J. Phys. Chem. 66*, 540−546.
23. Kay, L. E., Torchia, D. A., and Bax, A. (1989) Backbone dynamics of proteins as studied by ^{15}N inverse detected heteronuclear NMR spectroscopy: Application to staphylococcal nuclease, *Biochemistry 28*, 8972−8979.
24. Doig, A. J., and Sternberg, M. J. (1995) Side-chain conformational entropy in protein folding, *Protein Sci. 4*, 2247−2251.
25. Kay, L. E., Muhandiram, D. R., Farrow, N. A., Aubin, Y., and Forman-Kay, J. D. (1996) Correlation between dynamics and high affinity binding in an SH_2 domain interaction, *Biochemistry 35*, 361−368.
26. Nicholson, L. K., Kay, L. E., Baldisseri, D. M., Arango, J., Young, P. E., Bax, A., and Torchia, D. A. (1992) Dynamics of methyl groups in proteins as studied by proton-detected ^{13}C NMR spectroscopy. Application to the leucine residues of staphylococcal nuclease, *Biochemistry 31*, 5253−5263.
27. Lee, A. L., and Wand, A. J. (2001) Microscopic origins of entropy, heat capacity, and the glass transition in proteins, *Nature 411*, 501−504.
28. Slijper, M., Boelens, R., Davis, A. L., Konings, R. N. H., van der Marel, G. A., van Boom, J. H., and Kaptein, R. (1997) Backbone and side chain dynamics of *lac* repressor headpiece (1−56) and its complex with DNA, *Biochemistry 36*, 249−254.
29. Foster, M. P., Wuttke, D. S., Radhakrishnan, I., Case, D. A., Gottesfeld, J. M., and Wright, P. E. (1997) Domain packing and dynamics in the DNA complex of the N-terminal zinc fingers of TFIIIA, *Nat. Struct. Biol. 4*, 605−608.
30. Spolar, R. S., and Record, M. T., Jr. (1994) Coupling of local folding to site-specific binding of proteins to DNA, *Science 263*, 777.
31. Burgen, A. S., Roberts, G. C., and Feeney, J. (1975) Binding of flexible ligands to macromolecules, *Nature 253*, 753−755.
32. Tan, R., Chen, L., Buettner, J. A., Hudson, D., and Frankel, A. D. (1993) RNA recognition by an isolated α helix, *Cell 73*, 1031−1040.

BI048409E